We are IntechOpen, the world's leading publisher of Open Access books Built by scientists, for scientists

6,900
Open access books available

185,000
International authors and editors

200M
Downloads

Our authors are among the

154
Countries delivered to

TOP 1%
most cited scientists

12.2%
Contributors from top 500 universities



WEB OF SCIENCE™

Selection of our books indexed in the Book Citation Index in Web of Science™ Core Collection (BKCI)

Interested in publishing with us?
Contact book.department@intechopen.com

Numbers displayed above are based on latest data collected.
For more information visit www.intechopen.com



Chapter

Review on Metallization in Crystalline Silicon Solar Cells

Nagarajan Balaji, Mehul C. Raval and S. Saravanan

Abstract

Solar cell market is led by silicon photovoltaics and holds around 92% of the total market. Silicon solar cell fabrication process involves several critical steps which affects cell efficiency to large extent. This includes surface texturization, diffusion, antireflective coatings, and contact metallization. Among the critical processes, metallization is more significant. By optimizing contact metallization, electrical and optical losses of the solar cells can be reduced or controlled. Conventional and advanced silicon solar cell processes are discussed briefly. Subsequently, different metallization technologies used for front contacts in conventional silicon solar cells such as screen printing and nickel/copper plating are reviewed in detail. Rear metallization is important to improve efficiency in passivated emitter rear contact cells and interdigitated back contact cells. Current models on local Al contact formation in passivated emitter rear contact (PERC) cells are reviewed, and the influence of process parameters on the formation of local Al contacts is discussed. Also, the contact mechanism and the influence of metal contacts in interdigitated back contact (IBC) cells are reviewed briefly. The research highlights on metallization of conventional screen printed solar cells are compared with PERC and IBC cells.

Keywords: silicon solar cells, process flows, metallization, passivated emitter rear contact cells, interdigitated back contact cells

1. Introduction

The photovoltaic industry plays a critical part in the global energy scenario [1] to compete with the other renewable and conventional energy sources. Crystalline silicon (c-Si) wafer-based technologies [2, 3] dominate the photovoltaic market for terrestrial application due to its high efficiency, stability, and benefits arising out of microelectronic industry. Due to high production cost (i.e., high $/watt), researchers are continuously putting their efforts to improve low cost Si solar cell technology. Silicon solar cell fabrication process involves various vital steps [4, 5] which includes texturing [6], n+ and p+ diffusion [7, 8], antireflection coatings [9], and contact metallization [7–15]. Electrical parameters of the solar cell, namely open circuit voltage (V_{oc}), short circuit current (I_{sc}), and fill factor (FF) vary with processing conditions. Though the conventional Si processing technology is mature, it is important to modify fabrication process and device structure to improve electrical performance. Approaches such as nickel/copper metallization in conventional solar cell structure [16–18], passivated emitter rear contact (PERC) cells [19] and interdigitated back contacts (IBC) cells [20], etc. are being used in lab scale and production. In this chapter, contact mechanism in conventional structure and novel structures is reviewed.

2. Process flow and current status

Conventional silicon solar cell process and its current status in PV industry are discussed in detail. Subsequently, the process steps of advanced process techniques such as Ni/Cu plating-based silicon solar cell, PERC, and IBC are also discussed.

2.1 Conventional Si solar cell

Currently, most of the PV industries use boron-doped p-type wafers as the starting material for c-Si solar cell fabrication. The schematic diagram of conventional fabrication process is shown in **Figure 1**. As reported in [2, 21], every processing step contributes to losses in conventional screen printing solar cell. Screen printing metallization is cost-competitive and robust technology used in production. Screen printing technology has attracted considerable attention due to significant improvement in printing medium and simplicity of the process. Also, this technology increases the throughput and decreases the production cost. For metallization, several alternatives to screen printing are available to improve cell efficiency [22, 23]. However, the existing screen printing technology is the matured and cost effective technology [24, 25] compared to recently developed technologies such as PERC, IBC, and HIT. Hence, around 85% of Si solar cells are manufactured using screen printing of thick film pastes. In a typical solar cell process, screen printing has the potential to improve efficiency and lower the cost, since metallization pastes are continuously evolving and new generation of pastes are available.

In addition to the new generation pastes, the right choice of front grid design and screen pattern results in better efficiency with reduced cost. The new generation paste provided a better aspect ratio (the ratio of line height to line width). The improvement in the aspect ratio improves the current carrying capacity of the contacts, as the shadow loss is decreased as well as the series resistance also decreases. In addition to the paste rheology, enhancement of the aspect ratio relies on choosing the right screen parameters such as mesh count, wire dimension, and emulsion thickness. Along with the paste material, optimized screen parameters are also the important factors for making the front contact with high aspect ratio and reduced shadow loss, which are desired for getting high efficiency solar cells. The silicon solar cell researchers or industries have achieved a maximum efficiency of 19% on multicrystalline silicon and around 20% on mono crystalline silicon-based solar cells by using the conventional process as shown in **Figure 1** and are still working to enhance the efficiency using advanced materials.

Screen printing-based metallization technology occupies the significant role in solar cell manufacturing due to high throughput in cell production with better efficiencies. Though it is a mature technology, the finger aspects of the cells were limited by screen specifications and paste rheology.

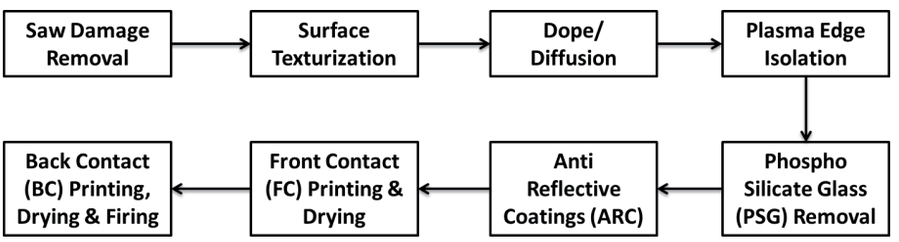


Figure 1.
Si solar cell process flow.

2.2 Ni/Cu metallization-based solar cell

The limitations of screen printing and chance of considering alternate materials for front contact led many researchers [26] to look for the Ni/Cu metallization-based cell process. It is observed that it is important to optimize the Ni/Cu metallization to compete with screen printing technology in terms of reliability, cost competitiveness, and high throughput production. Ni plating on solar cells started in 1959, and the process has been developed in subsequent years and came into the present process flow in early 1980s. Interdigitated back contact solar cells by Sun Power Corporation integrated metallization scheme of patterned Al followed by plated Ni—Cu—Ag which was further annealed to realize the contact [27] and its world record efficiency is 24% [28].

Table 1 shows the cost and properties comparison of copper (Cu), silver (Ag), and nickel (Ni). It can be seen that the resistivity of copper is only more by 3.7% as compared to Ag, while the cost being less by around a 100 times, which process to be an important factor for cost reduction. Moreover, Cu is widely used as interconnects in ultra-large-scale integrated circuits owing to its low resistivity and good resistance to electro migration and has a proven track record in the microelectronics industry. Hence, Cu is a possible choice for metallization of solar cells. The main drawback of Cu is its high mobility and being a highly reactive recombination center in silicon. This necessitates a diffusion barrier like Ni to prevent its diffusion in Si. The nickel silicide formed at the interface reduces the contact resistance, which will ensure minimum power loss due to series resistance (R_S) in a solar cell. Many groups have demonstrated cells based on Ni—Cu front side metallization with improved fill factor (FF) and higher efficiency (η) compared to Ag-based cells. The laser grooved buried contact (LGBC) technology utilizes Ni-Cu-based front-side metallization and has been successfully commercialized by BP Solar. The process flow of silicon solar cells with Ni/Cu front contact is shown in **Figure 2**.

One of the crucial steps in Ni/Cu metallization is opening of ARC to make selective contact with an emitter. Literatures reported for patterning ARC and subsequent metal deposition to make the front contact; however, it is important to choose the process which can compete with screen printing technology both in cost and performance. It has been found that one such a technique is Ni/Cu metallization which can be commercialized with few additional process steps. But in Ni/Cu metallization, it is

Parameters	Ag	Cu	Ni
Conductivity (10^6 S/m)	61.4	59.1	13.9
Density (gm/cm^3)	10.5	8.9	8.9
Typical cost ($/kg)	431.0	4.5	14.2

Table 1.
Cost and properties comparison of copper (Cu), silver (Ag), and nickel (Ni).

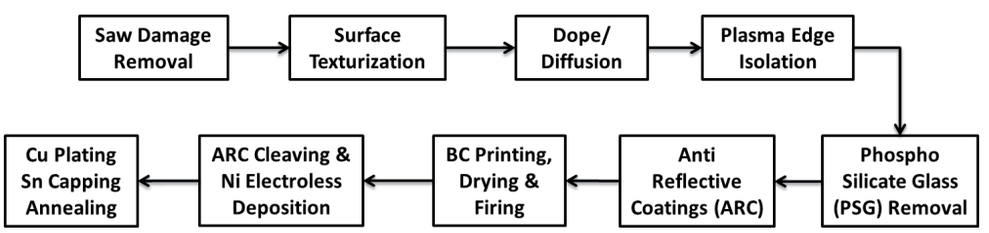


Figure 2.
Ni-Cu process flow.

Result type	Process difference	Substrate type	VOC (mV)	JSC (mA/cm^2)	FF (%)	η (%)
Best	Before LIP	mc-Si	612.1	34.6	74.9	15.9
Best	After LIP	mc-Si	613.4	34.1	79.2	16.6
Average	Before LIP	mc-Si	610.0 ± 2	34.5 ± 0.1	74.3 ± 0.6	15.6 ± 0.2
Average	After LIP	mc-Si	611.0 ± 2	34.1 ± 0.1	77.9 ± 0.9	16.3 ± 0.2
Best	Ni—Ni—Cu—Sn	Cz	619.0	35.7	72.7	16.4
Best	Ni—Cu—Sn	Cz	624.0	35.4	69.5	15.4
Best	Ni—Cu—Sn	Cz	623.0	37.3	74.2	17.2
Best	Background plating present	Cz	639.0	38.7	74.2	18.3
Best	No background plating	Cz	634.3	38.7	78.3	19.2
Best	—	Cz	638.3 ± 2	38.4 ± 0.7	78.8 ± 0.5	19.3 ± 0.4

Table 2.
Solar cell performance data for front contacts with electroplated metal layer(s).

important to standardize and optimize few critical parameters such as Ni thickness, annealing temperature for silicide formation, and Ni/Cu deposition parameters. The 80-μm thick stencil printed grid lines were thickened by electroplating of Ni—Cu—Sn stack with a commercial plating tool, improving the efficiency of the solar cells by 0.4% abs [29]. The platform had single side wafer processing and hence no chemical attack on the back side Al. Complete solar cell metallization based on electrochemical deposition of Ni and Cu has also been demonstrated [30]. Pulsed plating was used as compared to direct plating in the work to ensure homogeneous and well adhered contacts. LIP-based thickening of screen-printed contacts was first reported by Mette et al. [31]. An absolute η gain of 0.4% was obtained for large area cells based on standard production process, while an improvement of more than 1% absolute was possible for fine line 70-μm printed contacts. For an optimized grid design, an absolute η gain of 0.7% was achieved for large area cells as shown in **Table 2**. With an optimized SiN_x:H, η of 19.2% has been demonstrated on industrial grade Si with Ni and Cu layers deposited by LIP on LDSE cells [32]. pFF nearing 80% were possible with Ni—Cu—Sn-based contacts deposited by LIP, with no observable degradation in the pFF after a stress test at 200°C for 1000 hours.

After plating the conducting Cu layer, an Ag or Sn capping layer is deposited to protect the Cu conducting lines from oxidation and facilitate soldering of the interconnection tabs. Another important function of the capping layer is to prevent interaction of Cu with the EVA encapsulant. An impulse voltage test failure indicated by development of discharge sites was observed due to the presence of Cu particles at the Al/EVA interface on the back side [33]. Though the Ni—Cu contact-based LGBC cells were commercialized, low throughput rates and increased processing costs led to screen printed contacts becoming the standard for solar cell metallization [34]. Other major concern is regarding the chemical waste due to the metal baths which can lead to serious environment contamination issues [35]. Steady research and advances in plating techniques have enabled transition of solar cell with Ni—Cu-based metallization from labs to commercial scale production. Economic factors play vital role when considering an alternative technology with the introduction of new equipment in the fabrication line. As per the ITRPV roadmap, direct plating and plating on the seed layer are expected to have a share of around 15% in 2028 for the front-side metallization [36].

The Pluto series from Suntech Power is based on Ni—Cu metallization with stabilized efficiencies of 19.0% on large area mono-Si solar cells. There was an improvement of over 6% as compared to the screen printed contacts due to reduced shading and improvement in V_{OC}. IMEC has demonstrated conversion efficiencies of 20.3% on large area i-PERL cells with plated contacts. Using a PERC structure, Schott Solar along with Schmid Group demonstrated 20.9% efficient 6″ cells. Schott Solar has also demonstrated a median η of 20.8% with a best η of 21.3% on an industrial production line with electroplated contacts. Rena has recently demonstrated solar cells based on PERC technology reaching 20.8% with Ni—Cu metallization. Modules made with these cells successfully passed IEC 61215 test three times and adhesion of >1 N/mm. The technology can lead to a reduction in the cell production cost by $ 0.06.

Ni—Cu metallization yields the better efficiency compared to the conventional screen printing solar cells; however, due to the low throughput rates and increased processing costs, standard solar cell metallization dominates the PV industry. Also the chemical wastes of the metal baths in Ni—Cu metallization lead to environment disputes.

2.3 Passivated emitter rear contact solar cell

The conventional screen-printed Al-BSF cells suffer from the optical losses (front reflectance), transmission losses, and the recombination (rear side). The major limitation arises from the rear surface recombination which is due to the low solubility of Al in Si (doping concentration 7×10^{18} cm^3) during the very short firing process employed for alloying of screen printed Al paste. Though the boron co-doping with Al-BSF improves the doping concentration of Al-BSF [37, 38] owing to the higher solubility of boron, only 65% of the internally reflected longer wavelength light reaches the rear side, and hence the rear surface recombination is still being high [39]. One way to overcome the drawback of Al-BSF is the introduction of a dielectric rear side passivation with local contact points, which improves the optical properties with less surface recombination. One such cell architecture is the passivated emitter and rear cell [40]. With this structure, low rear surface recombination velocity of 60–200 cm^{-1} and internal reflectance over 95% have been realized so far. The dielectric passivation layer is locally opened for contact formation [40–47] by laser [48–50] or by printing etching pastes [51]. About 1% of the total rear surface is covered by the local point contacts. The local point contact is realized by photolithography in the laboratory level, and in mass production, the contacts are formed either by screen printed Al [38, 46, 47, 51–60] or by physical vapor deposition (PVD) of Al [40, 47]. The process flow for the PERC cell is shown in **Figure 3**. The key challenge in the local aluminum contact formation is that the Al should not be penetrated into the dielectric passivation layer [45]. The local Al-BSFs produced during the alloying process create voids below the Al contacts. These voids result in incomplete BSF formation and hence the rear surface recombination and contact resistances

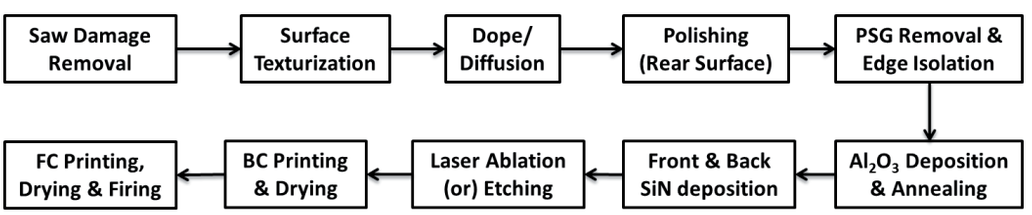


Figure 3.
PERC process flow.

are increased [38, 46, 47, 51–60]. An effective local Al-BSF is formed [61, 62] in the laser-fired contact process [63]. In this process, the deposition of the passivation layer followed by rear metallization (screen printed or evaporated contact) is carried out and finally with laser local contacts were formed. As a novel route, the rear Al electrode is formed by using commercial Al foil, thus complicated equipment such as evaporation or screen printing systems are avoided [64].

The best commercial PERC cell with 20–21% (mc-Si) and 21–22% (mono c-Si) has been achieved in the commercial scale [36]. A detailed investigation on the various factors involved in the formation of local Al contact formation and the influences of process steps have been studied by various authors and are described in the following sections. Meemongkolkiat et al. [52] observed that voids are created beneath the local Al contacts during the alloying process. Rauer et al. [38] avoided these voids by adding Si powder to the Al paste. The various factors that influence the contact formation are: (a) dielectric opening method, (b) rear-side contact geometry, (c) the amount of Al in the metallization paste, and (d) firing process.

2.3.1 Influence of process parameters on local-BSF formation

To form a high-quality localized contact, a deep Al-BSF is required for Al—Si contact interface to minimize the rear surface combination along with shunt free rear surface passivation. Urrejola [58] reported a shallow BSF or the presence of Kirkendall voids at the Al—Si interface as shown in **Figure 4**. **Figure 4(a)** shows the uniform BSF with a thickness of (4 μm). Void formation is due to sub-optimal conditions (**Figure 4(b)**) or inadequate BSF depth (**Figure 4(c** and **d)**). These voids reduce the FF as well as act as high recombination centers which affects J_{sc} and V_{oc}. Though the electrical contact is not affected with inadequate BSF depth, a very high contact recombination is expected. To minimize R_s with low contact resistivity, a very narrow local opening is required, hence high recombination beneath the metal contact is reduced. Urejola [56] obtained a lowest contact resistivity of 8 mΩ cm^2 for a shallow dielectric opening which lead to the FF loss minimization. However, narrow Al—Si alloy formation increases the dielectric passivated area under the contact, thus reducing J_{sc} and V_{oc}. The influence of contact size and finger spacing was investigated by Urejola [58]. The decrease in contact spacing reduced the overlap of Al on each side of the local opening leading to high quality BSF, thus lowering the presence of voids. For a contact spacing of 100 μm, the BSF thickness around 6–7 μm with less void (8%) was obtained. Similarly, Rauer et al. [38] concluded that the thickness of the local BSF depends on the contact spacing and obtained a BSF thickness up to 4 μm for a contact spacing of 400 μm. Further to increase the local BSF thickness and to avoid the void formation, the authors added more Si powder to the Al paste. This prevents the contact penetration into the Si bulk with enhanced Al-BSF thickness. Moreover, this increase in Si powder diminishes the emitter saturation current density (J_{0e}).

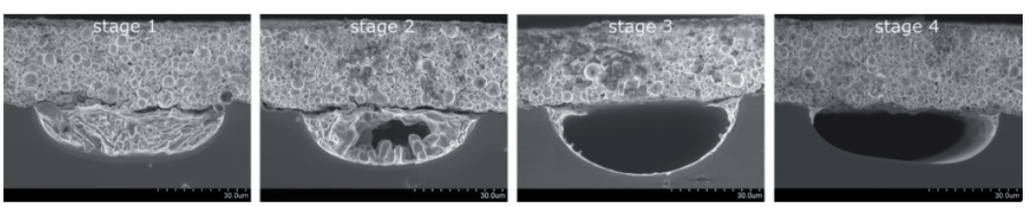


Figure 4.
The Al-Si interface showing (a) a well formed contact with deep BSF and no void formation, (b) a Kirkendall void, and (c) & (d) contact with shallow BSF [58].

2.3.2 Impact of dielectric opening method

A detailed investigation on the influence of formation of BSF using industrially screen printable local BSF Al paste and laser processing for removing the dielectric barrier was carried by Fang et al. and Bahr et al. [51, 53]. The laser ablation was carried out using nanosecond [wavelength (λ) = 1064 nm, pulse duration = 300ns, and pulse energy = <1.6 mJ] and femtosecond [wavelength (λ) = 1025 nm, pulse duration = 300fs and pulse energy = <36 μJ] laser. The ns laser has a strong influence on the local removing of the dielectric stack AlO_x/SiN_x:H, whereas fs showed a moderate influence. The strong and moderate influence is attributed to the interaction time between the laser pulse and the silicon substrate. With ns laser, few ten micrometer etching depth is achieved depending on the laser power, whereas in fs laser with very short interaction, few-micrometer depth is obtained. With screen printable local BSF Al etching paste, the passivation stack with 105 nm thick is etched off. After firing in an IR furnace with optimum belt speed, the local BSF formed with etching paste was more thicker (around 5 μm) and homogeneous with less voids. In the case of ns and fs, laser showed more voids with inhomogeneous thinner BSF (1–2 μm) due to the increased surface roughness.

2.3.3 Impact of contact resistivity

In recent days, the aluminum pastes are improved in such a way that even for thin laser contact opening (LCO), very low surface recombination is achievable. In future, decrease in the fraction of metallized area at the rear might is expected, hence R_s plays a vital role in the contact resistance of the Al—Si interface which is given by

$$R_{c,rear} = \rho_c / f_{rear} \quad (1)$$

where f_{rear} is the rear metallization fraction and ρ_c is the specific contact resistivity. However, ρ_c is independent of the contact size [65]. Similarly, Rohatgi et al. [66], on 2.3 Ω-cm wafers, obtained a ρ_c = 10 mΩ cm^2. Urrejola et al. [56] carried out the contact measurements with a PERC structure. The Al paste is printed on the top of the locally opened dielectric, and the transmission line model revealed the dependence of the ρ_c on the contact area. They obtained the ρ_c of 9–17 mΩ cm^2 for the dielectric opening width of 80–170 μm. Gatz et al. [67], to determine ρ_c, varied the rear contact pitch of PERC solar cells and obtained a ρ_c of 40–55 mΩ cm^2. The contribution of the bulk to the series resistance R_b is acquired either by calculation or numerical simulation. Kranz et al. [68] processed PERC-like TLM samples and measured the ρ_c of 3 mΩ cm^2, whereas the fit to the solar cell data resulted in ρ_c of 0.2–2 mΩ cm^2 and is shown in **Figure 5**.

2.3.4 PVD metallization

In most of the high efficiency solar cell concepts, the metallization is carried out using three different physical vapor deposition (PVD) techniques: sputtering, electron gun, and thermal evaporation. During the deposition of aluminum layer (2 μm), the substrate temperature increases to ~350°C, which mainly arises from the recrystallization heat of the aluminum. Comparing with the screen printing process, the mechanical and thermal impact on the wafer is substantially reduced. After the deposition of PVD aluminum layers, the contacts can be formed using laser pulses with different laser parameters which results in a much shallower profile. Hoffmann et al., on a 0.5 Ω cm p-type silicon, demonstrated a solar cell efficiencies up to 21.7% [69]. Reinwand et.al. [70] investigated PERC cells with

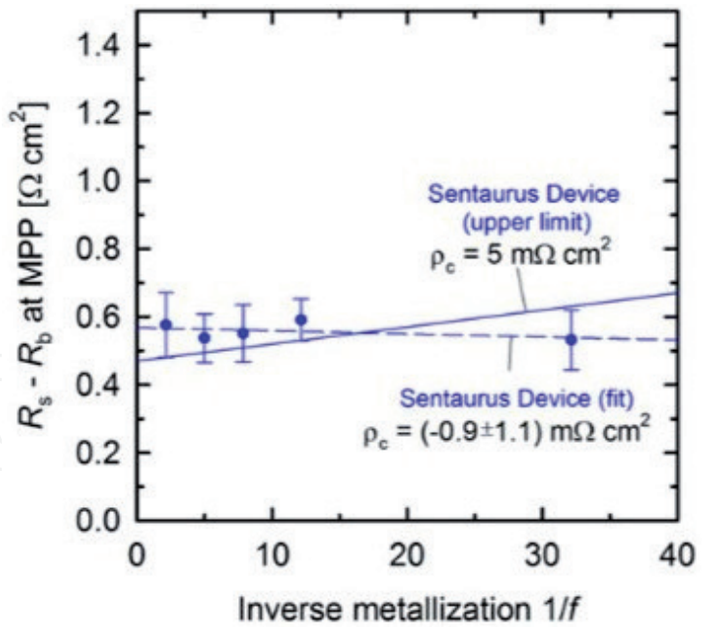


Figure 5.
Rs-Rb vs. inverse metallization fraction 1/f. Reproduced with permission from [68].

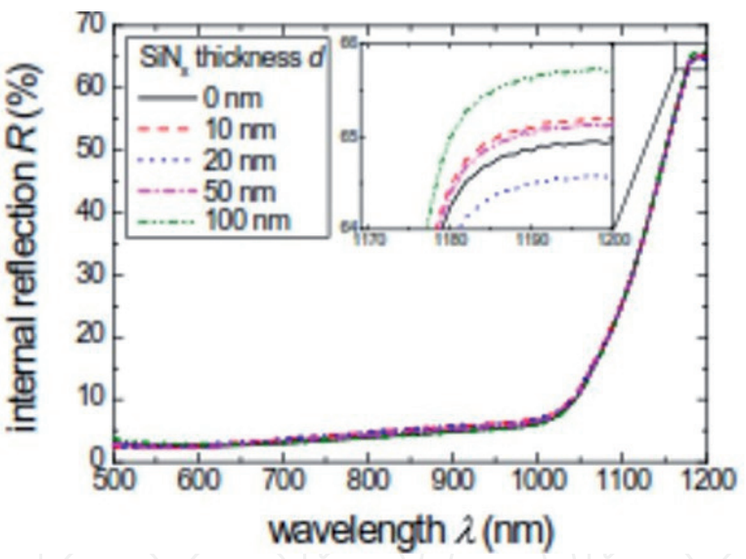


Figure 6.
Measurement of the internal reflection R at the rear side, after foil attachment and laser fired contacts dependent on the SiNx capping layer thickness. The reflection varies by < 0.5% in the IR regime [74].

sputtered aluminum on the rear side and a Ti—Ag (50/100 nm) seed layer on top prior to the silver plating. With the optimized annealing temperature, the highest efficiency η = 21.1 and 19.4% for FZ and CZ wafers, respectively, was determined with the lowest contact resistivity ρ_c = 0.36 mΩ cm^2.

2.3.5 Foil metallization

In 2007, researchers from F-ISE introduced the laser-based foil metallization technology called "FolMet." With this technology, the conventional aluminum foil is attached to the silicon wafer [71], and thus the laser fired contact process forms both the electrical contact at the rear side of PERC cell as well as the mechanical contact by locally melting the aluminum through the passivation layer into the bulk silicon [72]. The key advantages of this process is its enhanced internal optical

Issues	PVD	Screen print	Foil
Efficiency-potential	High	High	High
Flexibility	Medium	Low	High
Maturity	High	High	Low
Process temperature	300 °C	800–900°C	—
Cost	Medium	High	Low

Table 3.
Advantages and disadvantages of different printing mechanisms [75].

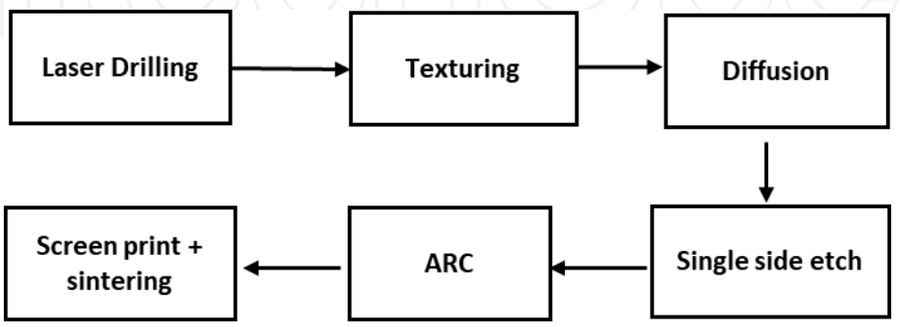


Figure 7.
Process flow of MWT PERC solar cells.

properties obtained due to the air gap between foil and passivation layer [73], cost reduction potential by decreasing the capping layer thickness, and ease of cell production process [74].

Figure 6 shows the internal reflection R at the rear side, after foil attachment and laser fired contacts. Nekarda et al., [73] by using the thick passivation layer optimized for the screen printed Al-paste, obtained an efficiency of 20.5%. In order to further reduce the cost, Graf et al. [74] adapted the rear side passivation layer with thinner capping layer and demonstrated an efficiency of 21.3% with a high J_{sc} due to the improved internal reflectance. Moreover, a low series resistance of 9 mΩ cm^2 of Al foil improved the FF to 80%. Pros and cons of various metallization schemes such as screen printing (SP), physical vapor deposition (PVD), and foil are tabulated in **Table 3**.

2.3.6 Metal wrap through PERC

MWT cell (**Figure 7**) is similar to the conventional solar cell design, and the external front contact busbars for interconnection are located at the rear side which increases J_{sc} due to the reduced shading loss. Lohmüller et al. [76], from FhG-ISE, combined the MWT concept (J_{sc} improvement) and passivated emitter rear contact (PERC) concept (reduced rear SRV) and reported a conversion efficiency of 18.7% with J_{sc} of 39.9 mA/cm^2, V_{oc} of 638 mV, and FF of 80.9% on a boron-doped p-type Cz grown silicon. The higher FF is due to the successful implementation of seed and plate technology [76]. Thaidigsmann from the same group introduced a simplified MWT-PERC cell called HIP-MWT (high performance metal wrap) to improve the efficiency by reducing the process complexity. In HIP-MWT structure, the formation of rear emitter is neglected hence no need of structuring steps. On a p-type FZ wafer with 0.5 Ω cm, a substrate thickness of 160 μm, on a cell area of 149 cm^2 resulted in an efficiency of 20.1% with J_{sc} of 39.1 mA/cm^2, V_{oc} of 659 mV, and FF of 77.8%, was obtained. The HIP-MWT cell demonstrated an efficiency of 19.6%

with J_{sc} of 40.2 mA/cm^2, V_{oc} of 649 mV, and FF of 75.1% on Cz grown wafer with 2.6 Ω cm for the same substrate thickness and cell area [77].

Passivated emitter rear contact solar cell with dielectric layer at the rear side and locally rear aluminum contacts reduces the recombination losses which increases the open circuit voltage. Also the rear dielectric layer increases the internal reflection and thus increases the current of the solar cell. Though the performance of PERC cell is better, the efficiency of PERC cell decreases after light-induced degradation which is around 0.5–1.0% absolute.

2.4 Interdigitated back contact solar cell

In IBC solar cells, optical shading loss is eliminated as both polarities of the metal contact are placed on the rear surface. In addition, the resistive power loss is reduced largely as the rear surface furnishes an opportunity for best design of metal contact formation. The other key advantages of IBC cell are (a) module manufacturing cost is reduced as the interconnection between the cells is simplified and (b) higher cell packing density increases the module power. The process flow of the IBC cell is shown in **Figure 8**. The major challenges present in the metallization of IBC cell includes: (i) shunting between the two polarities of metal contacts must be prevented and (ii) the metal conductors must be thick enough to ascertain the low resistive power loss. To isolate both the contacts, different cell-based metallization techniques can be used. One such method is patterning metal seed layer [78, 79], with electroplating to reduce resistance [80]. However, this plating up process needs electrical contact to the seed metal lines, which may lead to be problem with thinner wafers.

IBC solar cells with a record high efficiency of 25.6% were obtained by Sanyo/Panasonic [81], and the pioneer SunPower Corporation achieved 25% efficiency [82]. For IBC cells, the front surface field (FSF) reduces the surface recombination at the front as it acts as an electrical field which pushes back the minority carriers at the front surface [83]. The high expensive photolithography process is replaced with laser processing or screen printing which leads to a significant reduction in position accuracy which increases the pitch. This makes the majority carriers to travel from vertical to lateral direction. Depending on the pitch and base resistivity, series resistance over 90% contributing to the lateral majority carrier transport reduces the cell efficiency. Moreover the lateral majority carrier's current transport as well as the front surface passivation has been enhanced by FSF and finally the series resistance also significantly reduced to 0.1 and 1.3 Ω cm^2 for the base resistivity of 1 and 8 Ω cm, respectively, for the pitch of 3.5 mm [84].

The rear metallization of IBC cells is usually done with silver (Ag) and aluminum (Al) pastes [85], and Si/Ti/Pd/Ag or Si/Al/Ti/Pd/Ag metal stack and Al-deposited by PVD form a good ohmic contact with both n- and p-type silicon [86]. In Si/Ti/Pd/Ag or Si/Al/Ti/Pd/Ag metal stack, the Ag layer is used as a conductive layer because of its low resistivity. To avoid the reaction between Ti and Ag, the Pd layer is deposited between Ti and Ag layer. The work function of Ti or Al makes it suitable to contact with low contact resistivity [87] on both p- and n-doped

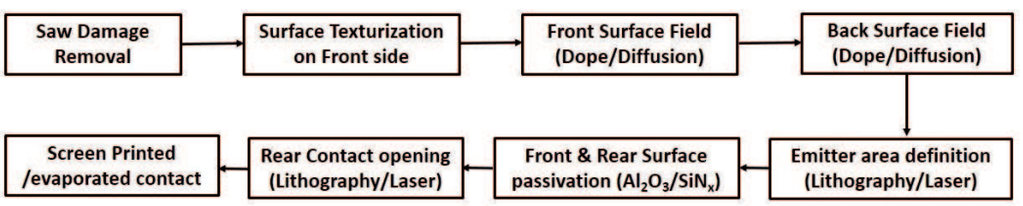


Figure 8.
IBC process flow.

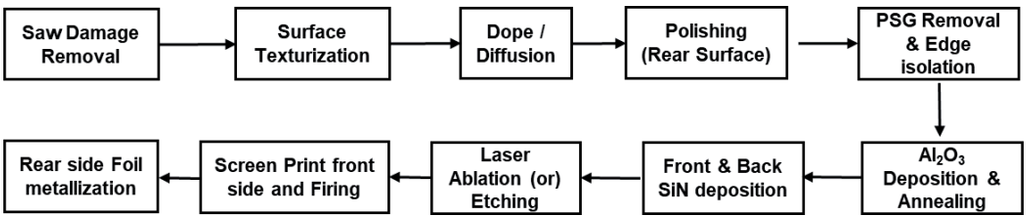


Figure 9.
Process flow of AMELI interconnection process.

regions. As Ti is a poor reflector, the Si/Al/Ti/Pd/Ag structure is adopted owing to the higher reflectance obtained with an Al layer which increases the light trapping. Couderca et al. [20] used Si/Ti/Ag stack with a thin Ti layer which has a low contact resistivity on both n- and p- doped regions. For n-doped surfaces, the specific resistivity is very low, and hence, the resistive losses are negligible. As the p-doped surfaces are lowly doped, the specific resistivity is higher though it stays under the crucial limit of 0.01 Ω cm^2. As a low-cost approach, Chena et al. [88] applied the aluminum electrodes deposited by e-beam evaporation using Al contact for high performance IBC cells. The specific contact resistivity of the Al contact cell resulted in 0.7 and 0.05 mΩ cm^2 on an n-doped and p-doped surface, respectively, and the final Al-contacted IBC cell resulted in an efficiency of 22.72%.

Recently, carrier selective contacts [TOPcon] using tunnel oxide and amorphous (a-Si) layer resulted in V_{oc} values around 720 mV and contact resistivities less than 10 mΩ cm^2 [89]. With poly-Si/SiO_x approach, similar values for their passivated contact have been achieved by various researchers [90–92]. Young et al. used the similar contact for the IBC solar cell patterned with ion implantation. The metallization layer consisting of thin Ti/Pd adhesion layer with 1-μm thick Ag layer and a Pd capping layer resulted in the contact resistivities less than 0.1 mΩ cm^2 [93].

Electrical shading loss plays a detrimental role as it reduces the collection efficiency of the minority carriers over the BSF regions [94], which compromises J_{sc}. By decreasing the width of the BSF region, this detrimental effect can be resolved. In the active cell area, by decreasing the finger pitch and BSF finger width, the electrical shading loss is minimized. Nevertheless, the base busbar still enforces electrical shading. In addition, as the majority carriers generated over the emitter busbar have to traverse over the entire wafer area, result in transport losses. The electrical shading loss and the transport loss contribute to the resistive losses and FF losses in the busbar metallization. Hence for further efficiency improvement, research group from ISFH developed a busbar less metallization which omits the busbar and eliminates the resistive losses in metallization with aluminum-based mechanical and electrical laser interconnection (AMELI) process for contacting aluminum-metalized IBC cells [95] and obtained a conversion efficiency of 22.1% with a V_{oc} of 683 mV, J_{sc} of 41.4 mA/cm^2, and FF of 78.1% on a cell area of 132 cm^2. AMELI process interconnects the solar cell with highly flexible interconnection geometry performed by a laser as structuring of the metallization. In addition, this AMELI process can interconnect that are as wide as the whole cell edge with a lower electrical resistance between the cells [96, 97]. **Figure 9** depicts the AMELI interconnection scheme for busbar-free solar cells. Woehl et al. introduced a point-shaped metalized IBC cells interconnected to a printed circuit board. The presence of only point-shaped metal contacts, increases the V_{oc} as the recombination area, is significantly reduced [98].

The main advantage of interdigitated back contact solar cells over other type of solar cells is zero shadow loss due to the absence of complete front contact. Although IBC is the high efficiency single junction cells among all other type of silicon solar cells, the carrier collection efficiency in front of the back surface field is low.

3. Conclusions

Process flows of conventional silicon solar cell, Ni/Cu plating for silicon solar cells, passivated emitter rear contact solar cells, and interdigitated back contact solar cells were discussed. Influences of process parameters in electrical parameters were analyzed. Though the contact formed by lithography, sputtering, etc. is reliable and resulting in good energy conversion efficiency, however, it is expensive due to the vacuum evaporation and single wafer type process. In this context, screen printed contacts are consistent in reliable and providing the best approach in production industry. Screen printing-based metallization is one of the key and crucial processes in silicon solar cell fabrication process which was discussed by interpreting the paste rheology, screen, and printing parameters. The screen printing paste used for contacting the solar cells is the other expensive element after the silicon wafer, and thus it is important to find an alternate technique for silver paste-based printing mechanism. Researchers arrived at a Ni/Cu plating technique for contact mechanism, and the technique has proved its capability in manufacturing industry as well. However, advanced structures such as PERC and IBC are using either screen printing or evaporation technique for making contacts. By seeing current scenario of metallization in different types of solar cells, it has been concluded that screen printing will continue to be an important and reliable metallization technique. The current efficiency status of different silicon solar cell technologies is depicted in **Table 4**.

S/N	Technology	Efficiency in %
1	Al BSF multi Si cell	19.0
2	Al BSF mono Si cell	20.0
3	Ni/Cu plating Si cell	21.3
4	PERC multi Si cell	22.0
5	PERC mono Si cell	25.0
6	MWT PERC Si cell	19.6
7	IBC Si cell	26.7

Table 4.
Current efficiency trend of different technology solar cells [36, 77, 99].

Acknowledgements

SS thanks the Management, RenewSys India Pvt. Ltd. and Faculties, National Centre for Photovoltaic Research and education, Indian Institute of Bombay, Mumbai for their support.

Disclaimer

The technical content in this article is the literature review of authors and do not necessarily reflect the official policy or position of RenewSys India Pvt. Ltd. Further, the authors hereby undertake to protect the proprietary technical and confidential information of RenewSys India Pvt. Ltd, including but not limited to the process parameters, recipes, formulations, sequences, methods, data, information etc. if any, referred in the above article, and have taken sufficient and appropriate measures and precaution to avoid the same from being inferred directly or indirectly in any manner whatsoever.

Definitions

V_{oc}	open circuit voltage
I_{sc}	short circuit current
J_{sc}	short circuit current density
J_{0e}	emitter saturation current density
FF	fill factor
R_s	series resistance
η	efficiency
ARC	anti-reflective coating
SP	screen printing
FSF	front surface field
AlBSF	aluminum back surface field
PERC	passivated emitter rear contact
IBC	interdigitated back contact
HIT	heterojunction with intrinsic thin layer
LGBC	laser grooved buried contacts
LIP	light induced plating
LDSE	laser-doped selective emitter
EVA	ethylene vinyl acetate
ITRPV	international technology roadmap for photovoltaic
i-PERL	passivated emitter with rear locally diffused
PVD	physical vapor deposition
LCO	laser contact opening
MWT	metal wrap through
HIP MWT	high performance metal wrap through
CZ	czochralski
FZ	float zone
SRV	surface recombination velocity
AMELI	aluminum based mechanical and electrical laser interconnection

IntechOpen

IntechOpen

Author details

Nagarajan Balaji[1], Mehul C. Raval[2] and S. Saravanan[3*]

1 Solar Energy Research Institute of Singapore (SERIS), Singapore

2 RCT Solutions GmbH Line - Eid, Konstanz, Germany

3 RenewSys India Pvt. Ltd, Hyderabad, India

*Address all correspondence to: shrisharavanan@yahoo.co.uk

IntechOpen

© 2019 The Author(s). Licensee IntechOpen. This chapter is distributed under the terms of the Creative Commons Attribution License (http://creativecommons.org/licenses/by/3.0), which permits unrestricted use, distribution, and reproduction in any medium, provided the original work is properly cited. CC BY

References

[1] Bolton JR. Solar cells—A technology assessment. Sol Energy. 1983;**31**: 483-502

[2] Koch W, Endros AL, Franke D, et al. Bulk crystal growth and wafering for PV. In: Luque A, Hegedus S, editors. Handbook of Photovoltaic Science and Engineering. 2nd ed. Chichester: John Wiley and Sons/Wiley; 2003. pp. 205-254

[3] Tobias I, del Canizo C, Alonso J. Crystalline silicon solar cells and modules. In: Luque A, Hegedus S, editors. Handbook of Photovoltaic Science and Engineering. 2nd ed. Chichester: John Wiley and Sons/Wiley; 2003. pp. 255-306

[4] Saravanan S, Meera M, Suratkar P, Gijo EV. Efficiency improvement on the multicrystalline silicon wafer through six sigma methodology. International Journal of Sustainable Energy. 2012;**31**:143-153

[5] Saravanan S, Suresh ChSR, Subraveti VV, Kumar KC, Jayaram UK. Effects of texture additive in large-area diamond wire cut multicrystalline silicon solar cells. Photovoltaics International. 2019;**42**:46-49

[6] Sankarasubramanian S, Saud GK, Shashikala M, Suratkar P, Saravanan S. Impact of surface texturization on overall performance of mono crystalline silicon solar cells. ECS Transactions. 2015;**66**:9-17

[7] Kumar D, Saravanan S, Suratkar P. Effect of oxygen ambient during phosphorous diffusion on silicon solar cell. Journal of Renewable and Sustainable Energy. 2012;**4**:33105-33113

[8] Guru Prasad A, Saravanan S, Gijo EV, et al. Six sigma approach on throughput improvement in the diffusion process of crystalline silicon solar cell manufacturing Int. International Journal of Sustainable Energy. 2016;**35**:190-204

[9] Guru Prasad A, Sreenivasa MD, Prakash S, Saravanan S. Effect of gas flow rates in optimizing silicon nitride films for large area multicrystalline silicon solar cells. International Journal of Electronics Letters. 2015;**3**:87-93

[10] Aakella PS, Saravanan S, Joshi SS, Solanki CS. Pre-metallization processes for c-Si solar cells. Solar Energy. 2013;**97**:388-397

[11] Coates K, Morrison S, Narayanan S, Madan A. Deposition of silicon nitride to improve the conversion efficiency of multicrystalline silicon solar cells. In: Proceedings of 16th EU PVSEC; Glasgow. 2000. pp. 1279-1281

[12] Hilali MM, Nakayashiki K, Khadilkar C, et al. Effect of Ag particle size in thick-film Ag paste on the electrical and physical properties of screen printed contacts and silicon solar cell. Journal of the Electrochemical Society. 2006;**153**:A5-A11

[13] Papet P, Nichiporuk O, Kaminski A, et al. Pyramidal texturing of silicon solar cell with TMAH chemical anisotropic etching. Solar Energy Materials & Solar Cells. 2006;**90**:2319-2328

[14] Park H, Kwon S, Lee JS, et al. Improvement on surface texturing of single crystalline silicon for solar cells by saw-damage etching using an acidic solution. Solar Energy Materials & Solar Cells. 2009;**93**:1773-1778

[15] Schultz O, Glunz SW, Riepe S, Willeke GP. High efficiency solar cells on phosphorus gettered multicrystalline silicon substrate. Progress in Photovoltaics: Research and Applications. 2006;**14**:711-719

[16] Mehul CR, Amruta PJ, Sandeep SS, Suckow S, Saravanan S, Solanki CS, et al. Study of nickel silicide formation and associated fill-factor loss analysis for silicon solar cells with plated Ni-Cu based metallization. IEEE Journal of Photovoltaics. 2015;**5**:1554-1562

[17] Mehul CR, Sandeep SS, Stephan S, Saravanan S, Solanki CS, Kottantharayil A. N_2O plasma treatment for minimization of background plating in silicon solar cells with Ni-Cu front side metallization. Solar Energy Materials & Solar Cells. 2016;**144**:671-677

[18] Jörg TH, Yuan S, Norbert B, et al. Industrial Si solar cells with Cu-based plated contacts. IEEE Journal of Photovoltaics. 2016;**5**:1595-1600

[19] Philipp RL, Gerd F, Lamine S, et al. Progress in fine-line metallization by co-extrusion printing on cast monosilicon PERC solar cells. Solar Energy Materials & Solar Cells. 2016;**142**:18-23

[20] Romain C, Mohamed A, Mustapha L.
Improvement of back surface metallization in a silicon interdigitated back contacts solar cell. Energy Procedia. 2013;**38**:684-690

[21] Green MA. Silicon Solar Cells: Advanced Principles and Practice. 2nd ed. Chichester: Wiley/Centre for Photovoltaic Devices and Systems; 1995

[22] Wenham SR, Green MA. Laser grooved solar cell. US Patent 4,626,613. 1986

[23] Ehling C, Schubert MB, Merz R, et al. 0.4% absolute efficiency gain by novel back contact. Solar Energy Materials & Solar Cells. 2009;**93**:707-709

[24] Denis E, Aleksander F, Marc R, et al. Advanced screen printing technique for high definition front side metallization of crystalline silicon solar cells. Solar Energy Materials & Solar Cells. 2010;**94**:57-61

[25] Dziedzic D, Nijs J, Szlufcik J. Thick-film fine-line fabrication techniques-application to front metallisation of solar cells. Microelectronics International. 1993;**10**(1):18-26

[26] Mehul CR, Chetan SS. Review of Ni-Cu based front side metallization for c-Si solar cells. Journal of Solar Energy. 2013. Article ID 183812. 20 pages

[27] Neuhaus DH, Munzer A. Industrial silicon wafer solar cells. Advances in Opto Electronics. 2007. Article ID 24521. 15 pages

[28] Content. 2013. Available from: http://us.sunpowercorp.com/

[29] Kuehnlein MBHH, Koesterke N, Cimiotti G, et al. >0.4% absolute efficiency gain by fast Ni-Cu-Sn electroplating of solar cells with fine line printed contacts by a single side wet treatment technology. In: Proceedings of 24th EU PVSEC. 2009. pp. 282-284

[30] Kroner F, Kroner Z, Reichmann K. All electrochemical layer deposition for crystalline silicon solar cell manufacturing: Experiments and interpretation. Solar Energy. 2012;**86**:548-557

[31] Mette AGWA, Schetter C, Wissen D, et al. Increasing the efficiency of screen-printed silicon solar cells by light-induced silver plating. In: Proceedings of IEEE 4th World Conference on Photovoltaic Energy Conference. 2006. pp. 1056-1059

[32] Lee E, Lee H, Choi J, et al. Improved LDSE processing for the avoidance of overplating yielding 19.2% efficiency on commercial grade crystalline Si solar cell. Solar Energy Materials & Solar Cells. 2011;**95**:3592-3595

[33] Gambogi WJ, McCord EF, Rosenfeld HD, et al. Failure analysis methods applied to PV module reliability. In: Proceedings of 24th EU PVSEC. 2009. pp. 3530-3534

[34] Hilali MM. Understanding and development of manufactuable screen-printed contacts on high sheet resistance emitters for low-cost solar cells [thesis]. Georgia Institute of Technology; 2005

[35] Ghannam M, Sivoththaman S, Poortmans J. Trends in industrial silicon solar cell processes. Sol Energy. 1997;**59**:101-110

[36] Fischer M. ITRPV 9th edition 2018 report release and key findings. In: PV Cell Tech conference. 2018

[37] Lolgen P, Sinke WC, Leguijt C, et al. Boron doping of silicon using coalloying with aluminium. Applied Physics Letters. 1994;**65**:2792

[38] Rauer M, Schmiga C, Woehl R, et al. Investigation of aluminum-alloyed local contacts for rear surface-passivated silicon solar cells. IEEE Journal of Photovoltaics. 2011;**1**:22-28

[39] Dong L, Malcolm A, Doris L, et al. Process optimization of localized BSF formation for solar cells with over 20% energy conversion efficiency. In: Proceedings of 40th IEEE PVSC. Denver; 2014. pp. 2503-2506

[40] Blakers AW, Wang A, Milne AM, et al. 22.8% efficienct silicon solar cell. Applied Physics Letters. 1989;**55**:1363-1365

[41] Dullweber T, Gatz S, Hannebauer H, et al. 19.4%-efficient large area rear-passivated screen printed silicon solar cells. In: Proceedings of 26th EU PVSEC. Hamburg; 2011. pp. 811-816

[42] Zielke D, Petermann JH, Werner F, et al. 21.7% efficient PERC solar cells with AlOx tunneling layer. In: Proceedings of 26th EU PVSEC. Hamburg; 2011. pp. 1115-1119

[43] Urrejola E, Petres R, Glatz-Reichenbach J, et al. High efficiency industrial PERC solar cells with all PECVD-based rear surface passivation. In: Proceedings of 26th EU PVSEC. Hamburg; 2011. pp. 2233-2235

[44] Choulat P, Agostinelli G, Ma Y, et al. Above 17% industrial type PERC solar cell on thin multicrystalline silicon substrate. In: Proceedings of 22nd EU PVSEC. Milan; 2007. pp. 1011-1014

[45] Agostinelli G, Szlufcick J, Choulat P, Beaucarne G. Local contact structures for industrial PERC-type solar cells. In: Proceedings of 20th EU PVSEC. Barcelona; 2005. pp. 942-945

[46] Lauermann T, Lüder T, Scholz S, et al. Enabling dielectric rear side passivation for industrial mass production by developing lean printing-based solar cell processes. In: Procedings of 35th IEEE PVSC. Honolulu; 2010. pp. 28-33

[47] Uruena A, John J, Beaucarne G, et al. Local Al-alloyed contacts for next generation Si solar cells. In: Proceedings of 24th EU PVSEC. Hamburg; 2009. pp. 1483-1486

[48] Metz A, Adler D, Bagus S, et al. Industrial high performance crystalline silicon solar cells and modules based on rear surface passivation technology. Solar Energy Materials & Solar Cells. 2014;**120**:417-425

[49] Münzer KA, Schöne J, Teppe A, et al. Towards 19.5% industrial crystalline silicon solar cells. In: Proceedings of 26th EUPVSEC. Hamburg; 2011. pp. 843-848

[50] Glunz SW, Preu R, Schaefer S, et al. New simplified methods for patterning the rear contact of RP-PERC high-efficiency solar cells. In: Proceedings

of 28th IEEE PVSC. Anchorage, Alaska; 2000. pp. 168-171

[51] Bahr M, Heinrich G, Doll O, et al. Differences of rear-contact formation between laser ablation and etching paste for PERC solar cells. In: Proceedings of 26th EU PVSEC. Hamburg; 2011. pp. 1203-1209

[52] Meemongkolkiat V, Nakayashiki K, Kim DS, et al. Investigation of modified screen-printing Al pastes for local back surface field formation. In: Proceedings of 4th WCPEC. Hawaii; 2006. pp. 1338-1341

[53] Fang T, Lin CM, Wang LT, Tang WC. Metallization of rear-side passivated solar cells: Reducing cavities on local contacts. In: Proceedings of 26th EU PVSEC. Hamburg; 2011. pp. 2220-2222

[54] Lauermann T, Zuschlag A, Scholz S, et al. Influence of the contact geometry and sub-contact passivation on the performance of screen printed Al_2O_3 passivated solar cells. In: Proceedings of 26th EU PVSEC. Hamburg; 2011. pp. 1137-1143

[55] Urrejola E, Peter K, Glatz-Reichenbach J, et al. Al-Si alloy formation in narrow p-Si contact areas. In: Proceedings of 2nd Metallization Workshop. Konstanz; 2010. pp. 11-14

[56] Urrejola E, Peter K, Plagwitz H, Schubert G. Al-Si alloy formation in narrow p-type Si contact areas for rear passivated solar cells. Journal of Applied Physics. 2010;**107**:124519

[57] Urrejola E, Peter K, Plagwitz H, Schubert G. Silicon diffusion in Aluminum for rear Passivated solar cells. Applied Physics Letters. 2011;**98**:153508

[58] Urrejola E, Peter K, Plagwitz H, Schubert G. Distribution of silicon in the aluminum matrix for rear passivated solar cells. Energy Procedia. 2011;**8**:331-336

[59] Urrejola E, Peter K, Plagwitz H, Schubert G. Effect of gravity on the microstructure of Al-Si alloy for rear-passivated solar cells. Journal of Applied Physics. 2011;**110**:056104

[60] Grasso FS, Gautero L, Rentsch J, Preu R, Lanzafame R. Characterisation of local Al-BSF formation for PERC solar cell structures. In: Proceedings of 25th EUPVSEC. Valencia; 2010. pp. 371-374

[61] Glunz SW, Schneiderlöchner E, Kray D, et al. Laser-fired contact solar cells on p- and n-type substrates. In: Proceedings of 19th EUPVSEC. Paris, France; 2004. pp. 408-411

[62] Kray D, Hermle M, Glunz SW. Theory and experiments on the back side reflectance of silicon wafer solar cells. Progress in Photovoltaics: Research and Applications. 2006;**14**:195

[63] Schneiderlochner E, Preu R, Ludemann R, Glunz SW. Laser-fired rear contacts for crystalline silicon solar cells. Progress in Photovoltaics: Research and Applications. 2002;**10**:29-34

[64] Nekarda JF, Lottspeich F, Wolf A, Preu R. Silicon solar cells using aluminum foil as rear side metallization reaching 21.0% efficiency. In: Proceedings of 25th EUPVSEC. Valencia; 2010. p. 2211

[65] Melczarsky M, Gallego GG, Posthuma N, et al. Contact resistance measurement techniques for Ag thick-film screen-printed contacts to solar cells. In: Proceedings of 34th IEEE Photovoltaic Spec. Conf. Philadelphia, PA; 2009. pp. 960-963

[66] Rohatgi A, Narasimha S, Ruby DS. Effective passivation of the low resistivity silicon surface by a rapid thermal oxide/PECVD silicon nitride stack and its application to passivated rear and bifacial Si solar cells. In: Proceedings of 2nd World Conference.

Photovoltaic Energy Conversion. Vienna, Austria; 1998. pp. 1566-1569

[67] Gatz S, Dullweber T, Brendel R. Evaluation of series resistance losses in screen-printed solar cells with local rear contacts. IEEE Journal of Photovoltaics. 2011;**1**:37-42

[68] Kranz C, Lim B, Baumann U, Dullweber T. Determination of the contact resistivity of screen-printed Al contacts formed by laser contact opening. Energy Procedia. 2015;**67**:64-69

[69] Hofmann M, Glunz SW, Preu R, Willeke G. 21%-efficient silicon solar cells using amorphous silicon rear side passivation. In: Proceedings of 21st EUPVSEC. Dresden, Germany; 2006. pp. 609-613

[70] Reinwand D, Specht J, Stüwe D, et al. 21.1% efficient PERC silicon solar cells on large scale by using inline sputtering for metallization. In: Proceedings of 35th IEEE Photovoltaic Specialists Conference (PVSC). Honulu; 2010. pp. 3582-3586

[71] Nekarda J, Grohe A, Schultz O, Preu R. Aluminum foil as back side metallization for LFC cells. In: Proceedings of 22nd EUPVSEC. 2007. pp. 1499-1501

[72] Schneiderlöchner E, Preu R, Lüdemann R, Glunz SW, Willeke G. Laser-fired contacts (LFC). In: Proceedings of 17th EUPVSEC. 2001. pp. 1303-1306

[73] Nekarda J, Graf M, Rodofili A, Preu R, Böhme R, Sontag D. Laser-based foil-metallization for industrial PERC solar cells. In: Proceedings of 28th EUPVSEC. 2013. pp. 797-799

[74] Graf M, Nekarda J, Eberlein D, Wöhrle N, Preu R, Böhme R, et al. Progress in laser-based foil metallization for industrial PERC solar cells. In: Proceedings of 29th EUPVSEC. 2014. pp. 532-535

[75] Nekarda J, Hörteis M, Lottspeich F, et al. Comparison of three different metallization concepts for LFC cells. In: Proceedings of 25th EUPVSEC. 2010. pp. 2245-2249

[76] Lohmüller E, Thaidigsmann B, Bartsch J, et al. Advanced metallization of rear surface passivated metal wrap through silicon solar cells. Energy Procedia. 2011;**8**:546-551

[77] Thaidigsmann B, Lohmüller E, Jäger U, et al. Large-area p-type HIP-MWT silicon solar cells with screen printed contacts exceeding 20% efficiency. Physica Status Solidi RRL: Rapid Research Letters. 2011;**5**:286-288

[78] Li Z, Cordiner D, Borojevic N, et al. Lift-off contact separation method for Interdigitated rear-contact solar cells. In: Proceedings of 21th International Photovoltaic Science and Engineering Conference. Fukuoka, Japan; 2011

[79] Mulligan WP, Cudzinovic MJ, Pass T, et al. Solar cell and method of manufacture. US Patent, US 7339,110 B. 2008

[80] Mir I, Kumar D. Recent advances in isotropic conductive adhesives for electronics packaging applications. International Journal of Adhesion and Adhesives. 2008;**28**:362-371

[81] Contents. Available from: http://news.panasonic.com/global/press/data/2014/04/en140410-4/en140410-4.html

[82] Smith DD, Cousins PJ, Masad A. SunPower's Maxeon gen III solar cell: High efficiency and energy yield. In: Proceedings of 39th IEEE PVSC. Tampa, FL; 2013

[83] Engelhart P, Harder NP, Grischke R, et al. Laser structuring for back

junction silicon solar cells. Progress in Photovoltaics: Research and Applications. 2007;**15**:237-243

[84] Granek F, Hermle M, Huljic DM, et al. Enhanced lateral current transport via the front N+ diffused layer of N-type high-efficiency back-junction back-contact silicon solar cells. Progress in Photovoltaics: Research and Applications. 2009;**17**:47-56

[85] Galbiati G, Mihailetchi VD, Roescu R, et al. Large-area back-contact back-junction solar cell with efficiency exceeding 21%. IEEE Journal of Photovoltaics. 2013;**3**:560-565

[86] Fong KC, Teng K, McIntosh KR, et al. Optimisation of n+ diffusion and contact size of IBC solar cells. In: Proceedings of 28th EU PVSEC. Paris; 2013

[87] Schroder D, Meier D. Solar cell contact resistance a review. IEEE Transactions on Electron Devices. 1984;**31**:637-646

[88] Chena Y, Yang Y, Zhang X, et al. Forming aluminum electrodes by screen printing and electron-beam evaporation for high performance interdigitated back contact solar cells. Solar Energy Materials & Solar Cells. 2015;**143**:205-211

[89] Feldmann F, Bivour M, Reichel C, Hermle M, Glunz SW. Passivated rear contacts for high-efficiency n-type Si solar cells providing high interface passivation quality and excellent transport characteristics. Solar Energy Materials & Solar Cells. 2014;**120**(A):270-274

[90] Romer U, Peibst R, Ohrdes T, et al. Recombination behavior and contact resistance of n+ and p+ poly-crystalline Si/mono-crystalline Si junctions. Solar Energy Materials & Solar Cells. 2014;**131**(A):85-91

[91] Upadhyaya A, Ok YW, Chang E, et al. Ion implanted screen printed N-type solar cell with tunnel oxide passivated back contact. In: Proceedings of 42nd IEEE Photovoltaic Specialists Conference. New Orleans, Louisiana; 2015

[92] Cuevas A, Allen T, Bullock J, et al. Skin care for healthy silicon solar cells. In: Proceedings of 42nd IEEE Photovoltaic Specialists Conference. New Orleans, Louisiana; 2015

[93] Young DL, Nemeth W, LaSalvia V, et al. Interdigitated back passivated contact (IBPC) solar cells formed by ion implantation. IEEE Journal of Photovoltaics. 2016;**8**:41-47

[94] Herme M, Granek F, Schultz-Wittmann O, Glunz SW. Shading effects in back junction back contacted silicon solar cells. In: Proceedings of 33rd IEEE PVSC. St. Diego, CA; 2008

[95] Schulte-Huxel H, Blankemeyer S, Merkle A, et al. Interconnection of busbar-free back contacted solar cells by laser welding. Progress in Photovoltaics: Research and Applications. 2015;**23**:1057-1065

[96] Schulte-Huxel H, Bock R, Blankemeyer S, et al. Aluminum-based mechanical and electrical laser interconnection process for module integration of silicon solar cells. IEEE Journal of Photovoltaics. 2012;**2**(1):16-21

[97] Schulte-Huxel H, Blankemeyer S, Bock R, et al. Aging behavior of laser welded Al-interconnections in crystalline silicon modules. Solar Energy Materials & Solar Cells. 2012;**106**:22-26

[98] Woehl R, Krause J, Granek F, Birot D. 19.7% efficient all-screen-printed back-contact back-junction silicon solar cell with aluminum-alloyed emitter. IEEE Electron Device Letters. 2011;**32**:345-347

[99] Green MA, Hishikawa Y, Dunlop ED, et al. Solar cell efficiency tables (version 53). Progress in Photovoltaics: Research and Applications. 2019;**27**:3-12